
Article:
Gawthrop, P.J., Wagg, D.J. and Neild, S.A. (2009) Bond graph based control and substructuring. Simulation Modelling Practice and Theory, 17 (1). 211 - 227. ISSN 1569-190X

https://doi.org/10.1016/j.simpat.2007.10.005

Bond Graph Based Control and Substructuring

P.J. Gawthrop [a,1] D.J. Wagg [b] S.A. Neild [b]

[a] *Centre for Systems and Control and Department of Mechanical Engineering, University of Glasgow, GLASGOW. G12 8QQ Scotland.*

[b] *Department of Mechanical Engineering, Queens Building, University of Bristol, Bristol BS8 1TR, UK.*

Abstract

A bond graph framework giving a unified treatment of both physical model based control and hybrid experimental-numerical simulation (also known as real-time dynamic substructuring) is given. The framework consists of two subsystems, one physical and one numerical, connected by a *transfer system* representing non-ideal actuators and sensors. Within this context, a two-stage design procedure is proposed: firstly, design and/or analysis of the numerical and physical subsystem interconnection as if the transfer system were not present; and secondly removal of as much as possible of the transfer system dynamics while having regard for the stability margins established in the first stage. The approach allows the use of engineering insight backed up by well-established control theory; a number of possibilities for each stage are given.

The approach is illustrated using two laboratory systems: an experimental mass-spring-damper substructured system and swing up and hold control of an inverted pendulum. Experimental results are provided in the latter case.

Key words: Bond graphs; physical-model based control; substructuring; hardware in loop simulation.

[1] Corresponding author. Email: P.Gawthrop@eng.gla.ac.uk

1 Introduction

Most research into control systems design is conducted in the *mathematical* domain. One reason for this is to abstract dynamic systems in such a way that control design is generic. For example, as described in elementary textbooks[9, 25], such system equations can be written in block diagram form for the purposes of control system design. However, it can be argued that this level of abstraction actually distills out system-specific features which could have aided the design procedure using engineering intuition. An alternative approach, "Design in the Physical Domain" has been suggested by Hogan [27, 28, 29] and Sharon, Hogan and Hardt[39]. Here the level of abstraction is a graphical physical representation which lies closer to the system physics than mathematical equations. In particular, the bond graph approach [5, 13, 20, 30, 34] has been suggested [12, 27, 28, 29, 39] as the basis for such design. Moreover, appropriate software tools are now available, including Model Transformation Tools (MTT) [33]. Following [12], we call this approach *Physical-model-based Control* (PMBC). Systems with *collocated* sensors and actuators can be easily controlled using such an approach [12].

However, in many cases, this collocation does not exist and the actual actuators and sensors are connected to notional collocated actuators and sensors by a *transfer system*[17, 18]. Such transfer systems typically contain small delays, high relative degree or unstable zero dynamics and are thus not passive.

Real-time dynamic *substructuring*[4] is a novel experimental testing technique which can be used to test individual components of engineering systems. This type of testing has been developed from experimental testing of large scale structures using extended time scales [8, 35]. The basic concept is that a complete model of the system is made by combining, in real-time, a part which is experimentally tested with a numerical model of the remainder of the system. In the fields of mechanical and aerospace engineering, physical components are often tested to either characterise or improve the design performance. Substructure testing offers a way of accurately testing nonlinear components as if they were in their operating environment. Some example applications are described in [44] in connection with aerospace engineering. Similarly, hardware-in-the-loop (HWiL) is a form of component testing where physical components of the system communicate with software models which simulate the behaviour of the rest of the system – a survey is given by [36]. For the purposes of this paper, HWiL testing and substructuring will be regarded as synonymous.

Once again, the issue of non-collocation due to the presence of a transfer system is the key issue. In particular, it has been shown [41, 42] that substructuring is sensitive to small time delays and methods have been developed to improve robustness [22].

Recently, the bond graph based virtual actuator approach [17], developed in the control systems context can also be applied to substructuring [23]. This paper brings together these results in a unifying bond graph framework. Moreover, a common framework for design and analysis is proposed which approaches the common problem of non-collocation due to the presence of a transfer system in a unified fashion. In particular, a two-step design procedure is proposed:

(1) Design the *collocated* feedback system using the standard approaches given above and analyse it using robustness methods drawn from feedback theory.
(2) Design a compensator to overcome the effect of the transfer system within the context of the robustness margins derived in step 1.

The formulation gives a new perspective on control design insofar as it focusses on the problems arising from non-collocation and also gives a new perspective on substructuring by reformulating the substructuring problem as a control problem.

We use two experimental systems to illustrate our approach: one is in the substructuring area and has been discussed previously[23], the other gives some new experimental results on the swing-up and hold control of an inverted pendulum – a system commonly used to evaluate control techniques[1, 31].

2 Physical Model Based Control and Substructuring

[Fig. 1 about here.]

The class of systems considered in this paper is represented by the bond graphs of Figure .1. There are three subsystems (themselves bond graphs) which represent:

Num the *numerical* subsystem implemented as *software* within a digital computer,
Phy the *physical* subsystem implemented as *hardware* in the physical world and
Tra the *transfer* system comprising sensors and actuators connecting the numerical and physical domains together with the associated control systems and signal conditioning.

The subsystems are connected by *power bonds* each of which carries an effort/flow pair[20, 30]. For example, the subsystem **Phy** is associated with the effort e_p and the flow f_p and the power flow $e_p f_p$. In general, the bonds could be *vector* bonds corresponding to the multiple connections; but this paper considers the scalar case. The subsystems could represent linear or nonlinear systems; again the focus is on the linear case although Section 4 considers a non-linear system.

The numerical subsystem **Num** exists in a digital computer and therfore does not actually transfer power; this is why the transfer system **Tra** is required to connect **Num** to **Phy**. Nevertheless, the equations describing **Num** are implemented in such

a way that a bond graph representation is applicable. There are practical issues concerning the numerical implementation of integration so that (simulated) energy is not dissipated [4]; but this is beyond the scope of this paper.

Figure 1(a) shows the ideal case where sensors and actuators are collocated. In particular, the both effort and flow associated with each subsystem are equal: $e_p = e_n$ and $f_p = f_n$. As discussed previously [12, 19], design is relatively straightforward in this case. In this paper, design and analysis of the collocated case is considered in section 2.1; in particular, the sensitivity of the feedback loop implied by the bond graph of 1(a) is analysed by classical methods.

In contrast, Figure 1(b) shows the non-collocated situation where $e_p \neq e_n$ and $f_p \neq f_n$ due to the presence of the transfer system **Tra**. In this situation, the approach of this paper is, having designed and analysed the collocated case, to remove the effect of the transfer system using an appropriate compensator. A number of possibilities are given in Section 2.2.

2.1 Collocated Design and Analysis

[Fig. 2 about here.]

[Fig. 3 about here.]

The physical subsystem **Phy** of Figure .1 has an energy port with the (collocated) covariables e_p and f_p connected to an energy port of **Num** with covariables e_n and f_n. In the case of PMBC, The design of a **Num** for such a feedback system can be accomplished by:

(1) physical insight [12, 27, 39] or
(2) dissipative system theory [26, 31, 43].

In the case of substructuring[4], the issue is to partition a physical system into **Num** and **Phy**[23].

Whatever method is used to overcome the dynamics of the transfer system (as discussed in Section 2.2), it is important to have a theoretical framework for evaluating, comparing and contrasting such methods. In particular, a successful control system must remain stable in the face of small errors in modelling or other neglected dynamics. For this reason, the sensitivity of the *collocated* design is considered first independently of the method used for transfer system elimination.

There are many methods available to analyse the robustness of feedback systems; here we illustrate our approach using the simplest transfer function based approach. The control literature contains many stability results based on transfer function

analysis; we use the recent textbook[25] as the reference for these. To use these transfer-function based methods causally complete versions of the bond graphs of Figure .1 must be used; in particular, there are two possibilities:

(1) *Effort actuation*. Effort is imposed by **Num** onto **Phy** via an ideal actuator (Figure 2(a)) and flow is imposed by **Phy** onto **Num** via an ideal sensor. As discussed by Hogan [27], this would naturally be used when the physical system is an *admittance* such as an *inertia* or bond graph **I** component.
(2) *Flow actuation*. The converse situation (Figure 2(b)) would naturally be used when the physical system is an *impedance* such as a *spring* or bond graph **C** component.

The following discussion is based on effort actuation (Figures 2(a) and 3(a)), but flow actuation (Figures 2(b) and 3(b)) can be considered with obvious modifications to the argument. The effort actuation is considered in the example of Section 3.2 (and the experimental results of Section 4), and flow actuation is considered in the example of Section 3.1.

The key insight is to realise that, following causal completion, the bond graph of Figure 1(a), representing the ideal system with no **Tra** dynamics, can be viewed as the *feedback loop* of Figure 3(a) where the transfer functions of **Num** and **Phy** (with effort actuation) are defined as $N(s) = N_f(s)$ and $P(s) = P_e(s)$ respectively where:

$$e_n = N(s) f_n \tag{1}$$
$$f_p = P(s) e_p \tag{2}$$

where $e_p = e_n$ if the system is ideal such that **Tra** may be neglected. Then the bond graph of Figure 2(a) can be transcribed as the conventional block diagram of Figure 3(a). Following standard control theory[25], and with reference to Figure 3(a), define the *loop-gain* transfer function $L(s)$ as

$$L(s) = -\frac{e_o}{e_i} = -N(s)P(s) \tag{3}$$

There are many ways of using $L(s)$ to investigate stability, but a simple one is using the concept of *phase margin* [25] which can be characterised as follows. Define the *critical frequency* ω_c as the solution of

$$|L(j\omega_c)| = 1, \tag{4}$$

The corresponding *phase margin* ϕ_m may be written as

$$\phi_m = \pi + \angle L(j\omega_c). \tag{5}$$

As discussed in the textbooks[25], the phase margin provides a measure of how near to instability the ideal system of 1(a) is in terms of how much phase lag (due to **Tra** and it's compensator) is permissible. Examples are given in Section 3.

2.2 Transfer system Compensation

Unfortunately, collocation is the exception rather than the rule. Figure 1(b) shows the practical situation where the computer imposes efforts or flows indirectly via an actuator/sensor system thus separating the measurement point from the actuation point leading to non-collocation. In this case, a compensation scheme must be designed to overcome some, or all, of the effects of **Tra**.

Once again, there are a number of well-established techniques that can be reused in this new context; some are from the control literature and some from the substructuring literature. Some possibilities are listed below and reinterpreted within the framework of this paper.

2.2.1 Impedance Control

[Fig. 4 about here.]

Hogan [27, 28, 29] introduced the concept of *impedance control* and applied it to the control of robotic manipulators interacting with their environment. A recent account point of view appears in Mukherjee et al. [34].

Figure .4 is a redrawn version of the summary of impedance control given in Figure 1 of [28]; **Z**:**Num** represents the desired impedance of the manipulator tip whereas **Y**:**Phy** represents the **admittance** of the environment with which the manipulator tip is in contact.

As discussed by Sharon et al. [39], impedance control is a special case of "design in the physical domain". In the context of this paper, comparison with Figure 1(a) reveals that, at this conceptual level, impedance control is a special case of the ideal physical-model based control & substructuring dealt with in this paper. In particular, **Num** of Figure 1(a) corresponds to the **Z**:**Num** and **0** junction portion of Figure .4 and **Phy** corresponds to the **Y**:**Phy** and **1** junction portion. The transfer system **Tra** of Figure 1(b) corresponds to the nonlinear dynamics of the manipulator; Hogan [27, 28, 29] shows how these dynamics can be removed in this particular case.

2.2.2 Virtual actuator control

The virtual actuator approach [17, 18] is a bond graph based approach to removing the transfer system by inversion by bond graph methods [16]. It is restricted to transfer systems with stable zero dynamics and relative degree restricted by the relative degree of the transfer system. It has been used in both control[17, 18] and substructuring[23] contexts.

2.2.3 Predictive control

It has become an accepted approach in the substructuring literature to approximate **Tra** by a pure time delay of Δs; that is with a transfer function:

$$T(s) = e^{-s\Delta} \tag{6}$$

See, for example, [2, 38, 42] and the references therein. These papers show that such a time-delay can be overcome by prediction of the signal by either extrapolation or by using a Smith predictor [32, 40].

This approximation has the advantage of simplicity, and captures the crucial phase lag of **Tra**. However, in many cases it is not a good approximation to a system that has, in fact, a transfer function that has a rational part (possibly coupled with a pure delay). This leads to the possibility that **Tra** has a combination of pure delay and phase effects, which appear to behave like a "frequency-dependent delay". To address this issue, methods of estimating the delay on-line have been developed to allow real-time adaptive delay compensation [7, 42]. A further extension to this method is to compensate for gain (amplitude) error via a second on-line identification and adaptation mechanism [42].

2.2.4 Emulator-based control

Emulator-based control (EBC) [10, 11, 14] provides a generalisation of Smith's predictor with a number of advantages. EBC can:

- successfully control systems with lightly-damped poles;
- explicitly account for the effect of measurement noise and
- handle more general forms of transfer system than Smith's predictor.

In particular, the EBC approach can be used to eliminate a transfer system containing both rational transfer function and pure time delay. Use of this approach in the substructuring context is a current reseach topic.

3 Illustrative Examples

The unifying approach of this paper is illustrated by two practical examples: a substructured mass-spring-damper system and the control of an inverted pendulum. In the substructuring example (Section 3.1), **Num** is the simulation of a part of a physical system; in the physical model based control example (Section 3.2) **Num** is a feedback controller (reprsented by a physical system). Thus these two examples emphasise the common framework of this paper.

3.1 Substructuring example

[Fig. 5 about here.]

The simple substructured system of Figure .5 has a numerical substructure consisting of a mass and linear damper and a physical substructure consisting of a linear spring. Although it is clear from physical reasoning that the substructured system is stable, this section shows that the phase-margin can be very small.

Using standard bond graph causality arguments [30], flow is imposed by **Num** onto **Phy** (via **Tra** - the actuator and its controller). The effort required to impose this flow on **Phy** is measured and fed back to **Num**. The resulting loop-gain is:

$$L(s) = \frac{k}{s(ms+c)} = \frac{\omega_n^2}{s(s+2\zeta\omega_n)} \tag{7}$$

where the natural frequency of the system of Figure .5 is $\omega_n = \sqrt{\frac{k}{m}}$ and the corresponding damping ratio $\zeta = \frac{c}{2m\omega_n}$. Defining $\lambda = \left(\frac{\omega_c}{\omega_n}\right)^2$ and using (4), the critical frequency corresponding to (7) is the solution of:

$$\lambda^2 + 4\zeta^2\lambda - 1 = 0 \tag{8}$$

The positive solution is:

$$\lambda = \sqrt{4\zeta^4 + 1} - 2\zeta^2 \tag{9}$$

Further analysis of (7) shows that the corresponding phase margin (5) is

$$\phi_m = 2\zeta\frac{\omega_n}{\omega_c} = \frac{2\zeta}{\sqrt{\lambda}} \tag{10}$$

[Fig. 6 about here.]

This simple system has the following properties:

- When $\zeta = 0$, $\omega_c = \omega_n$ and $\phi_m = 0$.
- For all ζ, the critical frequency ω_c is proportional to the natural frequency ω_n.
- For small ζ, $\omega_c \approx \omega_n$ and $\phi_m \approx 2\zeta\text{rad} \approx 100\zeta^\circ$.

A low damping ratio ζ of the substructured system of Figure .5 leads to a low phase margin. For example, if the neglected dynamics comprise a pure delay ($\Lambda(s) = e^{-s\tau}$) then the *critical delay*, τ_c, is the time delay which would give a phase lag of ϕ_m and is given by

$$\tau_c = \frac{\phi_m}{\omega_c}. \tag{11}$$

This system is thus sensitive to neglected time-delays; a result that had already been shown both experimentally and using the theory of delay-differential equations[41].

This small phase margin is typical of substructured systems where, as here, a lightly-damped resonance is created by the interconnection of the substructures. It is therefore vital to design the transfer system, **Tra**, (combining both physical systems associated control and instrumentation systems) to give $\Lambda(j\omega_c) \approx 1$ to give accurate and stable substructuring. A series of experiments reported elsewhere [23, 41, 42] have confirmed this predicted sensitivity analysis and emphasised the need for accurate cancellation of **Tra** around the critical frequency.

For these reasons, transfer system design in the context of substructuring is challenging and is the subject of current research; early attempts are considered elsewhere [24].

3.2 Physical model based control example

[Fig. 7 about here.]

[Table 1 about here.]

Figure 7(a) gives the schematic diagram of a control system designed in the physical domain and Figures 7(b) and 7(c) give the bond graphs of **Num** and **Phy** respectively. The left hand part of the diagram shows the spring-damper equivalent of a PI controller whilst the right hand part shows the mass-spring-damper system to be controlled. As discussed in Section 4.4, this is the linearised version of the inverted pendulum system. Design of this nominal system (that is Figure 1(a)) is simple; it merely involves choosing the controller spring and damper to give the desired closed-loop system – this is an illustration of the intuitive approach to collocated design.

[Fig. 8 about here.]

Table .1 gives the numerical values of the parameters of Figure .7; these correspond to the linearised inverted pendulum of Section 4 in the upright position. k_p is negative to reflect the destabilising effect of gravity, k_n is chosen to be $5|k_p|$ to overcome this. c_n is chosen to give critical damping. These values give the Nyquist plot of $L(j\omega)$ (Eq. (3)) shown in Figure .8. In this case, the phase-margin $\phi_m \approx 90^\circ$ indicating little sensitivity to the transfer system.

This large phase margin is in contrast to the small phase margin of the substructuring example of Section 3.1. The reason is that control systems, by their nature, are designed to *avoid* lightly-damped resonances arising from the connection of **Num** and **Phy**. Whereas, in substructuring, the properties of the numerical substructure **Num** may not be chosen – they are governed by the system being tested.

4 Experimental Inverted Pendulum

[Fig. 9 about here.]

The experimental equipment is based on the Quanser IP-02 "Self-erecting, Linear Motion, Inverted pendulum" experiment. Figure 9(a) shows a cart running on a horizontal track driven by a DC motor and the smaller gear wheel; the linear position y is measured by an encoder attached to the larger gear wheel. The pendulum is pivoted on an almost frictionless shaft and freely swings in the vertical plane; the angular position θ is measured by an encoder attached to the shaft. Figure 9(a) shows the cart and pendulum with the pendulum controlled in the up position ($\theta = \pi$).

The controller was implemented on a 2.66GHz Pentium P4 based processor on a AICMB800 motherboard with 512MB DRAM. The encoder signals and analogue output were handled by a Quanser MultiQ PCI-based data acquisition card. The software was built upon the Linux 2.4.20 kernel patched to support the Real-time Applications Interface (RTAI) version 24.1.11. This provides a hard real-time platform which in turn supports the Linux Control and Measurement Device Interface (COMEDI) version 0.7.66 and the corresponding library (comedilib) version 0.7.20 providing access to the data acquisition card and the Real Time Laboratory RTLab [6] providing a high-level programming interface together with archiving of experimental data.

The local and physical-model based controllers were implemented in C and compiled as a kernel module running in hard real time at 500Hz ($\Delta = 2$ ms) communicating with the data acquisition card via RTLab and Comedi and to a user interface module (programmed in C++ using the QT[37] library and running in user space) via shared memory. The non-linear controller code was automatically generated using MTT[33] as discussed elsewhere [3].

The three subsystems which make up the controlled inverted pendulum; the pendulum dynamics (**Phy**), the PMBC strategy (**Num**) and the transfer system (**Tra**) are now described in turn.

*4.1 Pendulum Dynamics (**Phy**)*

A number of authors (including [1]) have shown that the pendulum dynamics can be described by:

$$J\ddot{\theta} + mgl\sin\theta = T \tag{12}$$

$$T = ml\cos\theta\dot{v} = ml\cos\theta\ddot{y} \tag{13}$$

where v is the cart velocity, y is the cart position, J is the inertia of the pendulum about the pivot, θ is the pendulum angle measured clockwise from the downward position, m is the pendulum mass and l is the length of the pendulum from the pivot to the mass centre. T is the effective torque acting about the pendulum pivot. If the pendulum is a uniform rod, l is the pendulum half-length and $J = \frac{4}{3}ml^2$. Equation (12) corresponds to the bond graph of Figure 7(c) but with appropriate nonlinear constitutive relations (CR).

The second term of (12) ($mgl\sin\theta$) can be regarded as the result of a non-linear angular spring with linearised stiffness $K_g = mlg$Nm rad^{-1} about $\theta = 0$ (down) and $-K_g$ about $\theta = \pi$ (up). The first term ($J\ddot{\theta}$) is linear and corresponds to the rotational inertia J. The natural frequency of the free system linearised about $\theta = 0$ (down) is thus $\omega_n = \sqrt{\frac{K_g}{J}}$.

Control of the pendulum, (12), is achieved by applying the effective torque T to the pendulum pivot. This effective torque is calculated using a PMBC strategy in **Num** and is applied indirectly to the pendulum pivot via the motion of the cart, equation 13. In the PMBC design it is assumed that the acceleration of the cart may be applied to the system directly, as in figure 1(a). In the real system there are some dynamics associated with the generation of the cart acceleration — **Tra**. The elimination of **Tra** is discussed in Section 4.3.

*4.2 Pendulum Control Design (**Num**)*

With reference to Figure 9(b), and as discussed in Section 3.2, an appropriate physically based control is to append a rotational spring K and a rotational damper R to the pendulum in such a way as to complement these natural properties of the unforced system. This is shown in the bond graph of Figure 7(b) which again has appropriate non-linear CRs.

In the experiments reported here, the additional spring is chosen so that its linearised stiffness in the up position K_u and down position K_d are given by

$$K_u = (k_u + 1)K_g;\ K_d = (k_d - 1)K_g \tag{14}$$

Thus the net stiffness of the spring and gravity is k_uK_g and k_dK_g in the up and down positions respectively. Similarly, the additional damper R is chosen so that in the up and down positions the linearised damping ratio is ζ_u and ζ_d by choosing the linearised damping coefficient in the up and down positions to be:

$$R_u = 2\omega_u J\zeta_u;\ R_d = 2\omega_d J\zeta_d \tag{15}$$

where the up and down natural frequencies are

$$\omega_u = \sqrt{\frac{K_u}{J}};\ \omega_d = \sqrt{\frac{K_d}{J}} \tag{16}$$

There are many possible functions which have these linearised properties, but there are two facts that need to be considered.

(1) (13) contains a factor $\cos\theta$; it is better to work with this factor than to attempt to cancel it. In particular, when the pendulum is horizontal ($\theta = \frac{\pi}{2}$), $\cos\theta = 0$ and cannot be cancelled. On the other hand, at this angle, the cart has no effect on the pendulum angle so there is no point in trying to apply a control signal.
(2) Non-zero T implies an accelerating cart position y which can lead to the cart reaching the end of its track.

The first is taken care of by including a $\cos^2\theta$ in the CR, the squaring not changing the overall sign of the CR; the second by using a "selection" function $S(\theta)$ which avoids control action away from the up and down positions.

[Table 2 about here.]

Taking into account these factors, in the experiments reported here, the following constitutive relations (CR) were used for the virtual spring and damper:

$$T = K(\theta) + R(\theta)\dot{\theta} \tag{17}$$
$$K(\theta) = S(\theta)\cos^2\theta(K_0 + K_1\cos\theta)\sin\theta \tag{18}$$
$$R(\theta) = S(\theta)\cos^2\theta(R_0 + R_1\cos\theta) \tag{19}$$
$$K_0 = (K_d - K_u)/2;\ K_1 = (K_d + K_u)/2 \tag{20}$$
$$R_0 = (R_d + R_u)/2;\ R_1 = (R_d - R_u)/2 \tag{21}$$
$$S(\theta) = \frac{1}{2}[1 + \tanh(\alpha(\cos(2\theta) - \cos(2\theta_0)))] \tag{22}$$

Equations (18) and (19) account for item 1; equation (22) accounts for item 2. The parameters of Table .2 were used.

Although the linear analysis of Section 3.2 is not applicable to this nonlinear system, it is applicable to the linearisation about the vertical (unstable) equilibrium.

*4.3 Transfer system (**Tra**) design and compensation*

[Fig. 10 about here.]

[Table 3 about here.]

As discussed in Section 4.1, the transfer system output corresponds to cart *acceleration* $\dot{v}$. The cart shown in Figure 9(a) contains a DC motor driven from an external power supply. Because it is important to have a tightly controlled transfer system, an inner loop provides accurate control of cart linear velocity $v = \dot{y}$ to give a well-defined transfer function between velocity setpoint w and velocity v as well as to reject disturbances due to the motion of the pendulum.

The resultant cart dynamics, together with the control system, are simplified and become the transfer system of Figures 10(a) and 10(b),

$$\frac{\dot{v}}{w} = T(s) = \frac{r_1 s}{r_1 + r_2 + Ms} \tag{23}$$

Only two of the three parameters (r_1,r_2 and M) appearing in (23) are independent, so M is chosen to be the actual mass of the cart - an easily measured quantity which is given in the experimental manual. The physical-model based identification approach of Gawthrop [15] was used to identify the remaining unknown parameters r_1 and r_2; the results appear in Table .3.

The inverse of this transfer function is proper and thus the inner-loop setpoint w can be directly generated from $\frac{1}{T(s)}$. This is a special case of the virtual actuator approach[17, 18, 21]. As the collocated design has a large phase margin, the values used in (23) are not critical.

4.4 Experimental Results

[Fig. 11 about here.]

[Fig. 12 about here.]

The physical system of Figure 9(b) was simulated from $t = 0$ to $t = 25$s with initial conditions $\theta = 0.1\pi$,$\dot{\theta} = 0$, using implicit Euler integration with a step of 0.01s and the model described by (12)–(22) with the numerical parameters of Table .2. The results are shown in Figure .11. A number of experiments were performed. In each case, the experiment was set swinging manually by a sideways tap in the down position. One set of results appear in Figure .12. The simulation and experiment results are described for each sub-figure.

(a) The normalised pendulum angle $\frac{\theta}{2\pi}$ is plotted against time. It starts at the initial condition (almost down) and ends up at $\theta = -\pi$, i.e. vertically up. The non-zero initial condition is necessary to avoid the (closed-loop) unstable equilibrium at $\theta = 0$. The simulation (Figure 11(a)) and experimental (Figure 12(a)) results are similar in form with about one swing per second. The exper-

iment takes about 10 swings to the up position as opposed to about 13 in the simulation; this discrepancy is attributed to different initial conditions.

(b) The normalised angular velocity $\frac{\dot{\theta}}{2\pi}$ is plotted against normalised pendulum angle $\frac{\theta}{2\pi}$ to give a phase-plane portrait. The trajectory spirals out from near the origin and ends at $\theta = -\pi$ and $\dot{\theta} = 0$. The distortion around the line $\theta = 0$ corresponds to the negative damping at this point. The simulation (Figure 11(b)) and experimental (Figure 12(b)) results are similar.

(c) Cart position y is plotted against time. The amplitude of cart movement is small compared to the overall track length of about 1m. In the simulation (and some experiments not shown) the cart has a tendency to drift; the amount of drift depends on initial conditions. It happens to be different in simulation and experiment because the initial conditions are not the same.

(d) The cart velocity $v = \dot{y}$ and corresponding setpoint w are shown for the simulation (Figure 11(d)) and experiment (Figure 12(d)). In each case, the inner loop ensures that the error is small. The "spikes" in velocity correspond to $\theta = 0$, giving a cart acceleration (and effective torque) corresponding to the non-linear damping. The constant velocity in between the spikes corresponds to zero acceleration and zero effective torque. The final part of Figure 12(d) exhibits the effect of measurement noise.

5 Conclusion

A unified approach to physical model based control and substructuring has been given and the corresponding two-stage design method has been illustrated. This novel framework allows well-established control methods to be used in a new context to provide an intuitively-motivated approach to control and substructuring to be built on firm foundations.

The use of a bond graph formulation clarifies the issue of collocation and, particularly in the case of substructuring, clarifies issues of causality. The notion of a transfer system clarifies the key issues of non-collocation.

Future work will consider multivariable, non-linear and adaptive extensions to the theory together with practical applications.

6 Acknowledgements

The experimental work on the inverted pendulum was accomplished while the first author was a Visiting Professor at the University of New South Wales within the Systems and Control Research Group of the School of Electrical Engineering &

Telecommunications. The comedi driver (multiqpci.c) reffered to in Section 4 was written by Linh Vu at UNSW and modified by the first author. The real-time software RTLab is part of an Open Source project developed by David Christini and Calin Culianu of Cornell University funded by NSF grant DBI-0096596. This research was partially funded by the Royal Academy of Engineering under International Travel Grants ITG 04-311 and ITG 05-280. Max Wallace developed and successfully controlled the substructuring experiment whilst sponsored by and EPSRC DTA. David Wagg is supported by an EPSRC ARF.

References

[1] K.J. Åström and K. Furuta. Swinging up a pendulum by energy control. *Automatica*, 36:287–295, 2000.

[2] A.K. Agrawal and J.N. Yang. Compensation of time-delay for control of civil engineering structures. *Earthquake Engng Struc. Dyn.*, 29(1):37–62, January 2000.

[3] Donald J. Ballance, Geraint P. Bevan, Peter J. Gawthrop, and Dominic J. Diston. Model transformation tools (MTT): The open source bond graph project. Submitted to ICBGM '05, July 2004.

[4] A. Blakeborough, M.S. Williams, A.P. Darby, and D.M. Williams. The development of real-time substructure testing. *Philosophical Transactions of the Royal Society pt. A*, 359(1869-1891), 2001.

[5] F. E. Cellier. *Continuous system modelling*. Springer-Verlag, 1991.

[6] David Christini and Calin Culianu. RTLab. Online WWW Home Page, 2003. URL: http://www.rtlab.org.

[7] A.P. Darby, M.S. Williams, and A. Blakeborough. Stability and delay compensation for real-time substructure testing. *ASCE Journal of Engineering Mechanics*, 128(12):1276–1284, 2002.

[8] J. Donea, P. Magonette, P. Negro, P. Pegon, A. Pinto, and G. Verzeletti. Pseudodynamic capabilities of the elsa laboratory for earthquake testing of large structures. *Earthquake Spectra*, 12(1):163–180, 1996.

[9] R. G. Dorf. *Modern Control Systems*. Addison-Wesley, 1980.

[10] P. J. Gawthrop. *Continuous-time Self-tuning Control. Vol 1: Design*. Research Studies Press, Engineering control series., Lechworth, England., 1987.

[11] P. J. Gawthrop. *Continuous-time Self-tuning Control. Vol 2: Implementation*. Research Studies Press, Engineering control series., Taunton, England., 1990.

[12] P. J. Gawthrop. Physical model-based control: A bond graph approach. *Journal of the Franklin Institute*, 332B(3):285–305, 1995. URL `http://dx.doi.org/10.1016/0016-0032(95)00044-5`.

[13] P. J. Gawthrop and L. P. S. Smith. *Metamodelling: Bond Graphs and Dynamic Systems*. Prentice Hall, Hemel Hempstead, Herts, England., 1996. ISBN 0-13-489824-9.

[14] P. J. Gawthrop, Jones, R. W., and D. G. Sbarbaro. Emulator-based

control and internal model control: Complementary approaches to robust control design. *Automatica*, 32(8):1223–1227, August 1996. URL http://dx.doi.org/doi:10.1016/0005-1098(96)00059-3.

[15] Peter J Gawthrop. Sensitivity bond graphs. *Journal of the Franklin Institute*, 337(7):907–922, November 2000. URL http://dx.doi.org/10.1016/S0016-0032(00)00052-1.

[16] Peter J Gawthrop. Physical interpretation of inverse dynamics using bicausal bond graphs. *Journal of the Franklin Institute*, 337(6):743–769, 2000. URL http://dx.doi.org/10.1016/S0016-0032(00)00051-X.

[17] Peter J Gawthrop. Bond graph based control using virtual actuators. *Proceedings of the Institution of Mechanical Engineers Pt. I: Journal of Systems and Control Engineering*, 218(4):251–268, September 2004. URL http://dx.doi.org/10.1243/095965104116586 4.

[18] Peter J Gawthrop. Virtual actuators with virtual sensors. *Proceedings of the Institution of Mechanical Engineers Pt. I: Journal of Systems and Control Engineering*, 219(5):371 – 377, August 2005. URL http://dx.doi.org/10.1243/095965105X33473.

[19] Peter J. Gawthrop and Donald J. Ballance. Symbolic algebra and physical-model-based control. *Computing and Control Journal*, 8(2):70–76, April 1997. ISSN 0956-3385.

[20] Peter J Gawthrop and Geraint P Bevan. Bond-graph modeling: A tutorial introduction for control engineers. *IEEE Control Systems Magazine*, 27(2): 24–45, April 2007.

[21] Peter J Gawthrop, Donald J Ballance, and Dustin Vink. Bond graph based control with virtual actuators. In Norbert Giambiasi and Cluadia Frydman, editors, *Proceedings of the 13th European Simulation Symposium: Simulation in Industry*, pages 813–817, Marseille, France, October 2001. SCS. ISBN 90-77039-02-3.

[22] P.J. Gawthrop, M.I. Wallace, S.A. Neild, and D.J. Wagg. Robust real-time substructuring techniques for under-damped systems. Submitted to Structural Control and Health Monitoring, June 2005.

[23] P.J. Gawthrop, M.I. Wallace, and D.J. Wagg. Bond-graph based substructuring of dynamical systems. *Earthquake Engng Struc. Dyn.*, 34(6):687–703, May 2005. URL http://dx.doi.org/10.1002/eqe.450.

[24] P.J. Gawthrop, M.I. Wallace, S.A. Neild, and D.J. Wagg. Robust real-time substructuring techniques for under-damped systems. *Structural Control and Health Monitoring*, 14(4):591–608, June 2007. URL http://dx.doi.org/10.1002/stc.174. Published on-line: 19 May 2006.

[25] G.C. Goodwin, S.F. Graebe, and M.E. Salgado. *Control System Design*. Prentice Hall, 2001.

[26] David J. Hill and Peter J. Moylan. Dissipative dynamical systems: Basic input-output and state properties. *Journal of the Franklin Institute*, 208(5): 327–357, 1980.

[27] N. Hogan. Impedance control: An approach to manipulation. part I–theory.

ASME Journal of Dynamic Systems, Measurement and Control, 107:1–7, March 1985.

[28] N. Hogan. Impedance control: An approach to manipulation. part II–implementation. *ASME Journal of Dynamic Systems, Measurement and Control*, 107:8–16, March 1985.

[29] N. Hogan. Impedance control: An approach to manipulation. part III–applications. *ASME Journal of Dynamic Systems, Measurement and Control*, 107:17–24, March 1985.

[30] Dean Karnopp, Donald L. Margolis, and Ronald C. Rosenberg. *System Dynamics : Modeling and Simulation of Mechatronic Systems*. Horizon Publishers and Distributors Inc, 3rd edition, January 2000.

[31] R. Lozano, B. Brogliato, O. Egelund, and B. Maschke. *Dissipative systems: analysis and control*. Springer, 2000.

[32] J. E. Marshall. *Control of Time-delay Systems*. Peter Peregrinus, 1979.

[33] MTT. MTT: Model transformation tools. Online WWW Home Page, 2002. URL: http://mtt.sourceforge.net.

[34] A. Mukherjee, R. Karmakar, and A.K. Samantaray. *Bond Graph in Modeling, Simulation and Fault Detection*. I.K. International Publishing, New Delhi, 2006.

[35] M. Nakashima, H. Kato, and E. Takaoka. Development of real-time pseudo dynamic testing. *Earthquake Engineering and Structural Dynamics*, 21:779–92, 1992.

[36] A.R. Plummer. Model-in-the-loop testing. *Proceedings of the Institution of Mechanical Engineers, Part I: Journal of Systems and Control Engineering*, 2006. (accepted).

[37] QT. QT. Online WWW Home Page, 2004. URL: http://www.trolltech.com/.

[38] A.M. Reinhorn, M.V. Sivaselvan, Z. Liang, and X. Shao. Real-time dynamic hybrid testing of structural systems. In *Thirteenth World Conference on Earthquake Engineering*, Vancouver, August 2004. Paper No 1644.

[39] A. Sharon, N. Hogan, and D. E. Hardt. Controller design in the physical domain. *Journal of the Franklin Institute*, 328(5):697–721, 1991.

[40] O. J. M. Smith. A controller to overcome dead-time. *ISA Transactions*, 6(2): 28–33, 1959.

[41] M.I. Wallace, J. Sieber, S.A. Neild, D.J. Wagg, and B. Krauskopf. A delay differential equation approach to real-time dynamic substructuring. *Earthquake Engng Struc. Dyn.*, 34(15):1817 – 1832, 2005. URL `http://dx.doi.org/10.1002/eqe.513`.

[42] M.I. Wallace, D.J. Wagg, and S.A. Neild. An adaptive polynomial based forward prediction algorithm for multi-actuator real-time dynamic substructuring. *Proceedings of the Royal Society*, 461(2064):3807 – 3826, December 2005. URL `http://dx.doi.org/10.1098/rspa.2005.1532`.

[43] J. C. Willems. Dissipative dynamical systems, part I: General theory, part II: Linear system with quadratic supply rates. *Arch. Rational Mechanics and Analysis*, 45(5):321–392, 1972.

[44] M. S. Williams and A. Blakeborough. Laboratory testing of structures under

dynamic loads: an introductory review. *Philosophical Transactions of the Royal Society A*, 359:1651 – 1669, 2001.

List of Figures

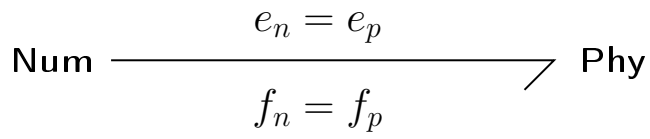

(a)

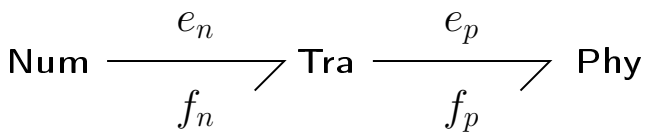

(b)

Fig. .1. Physical Model Based Control and Substructuring. (a) Ideal, (b) Actual. In these acausal diagrams, there is no implication as to whether e_n causes e_p (or f_n causes f_p) or vice-versa. Figure .2 considers causality.

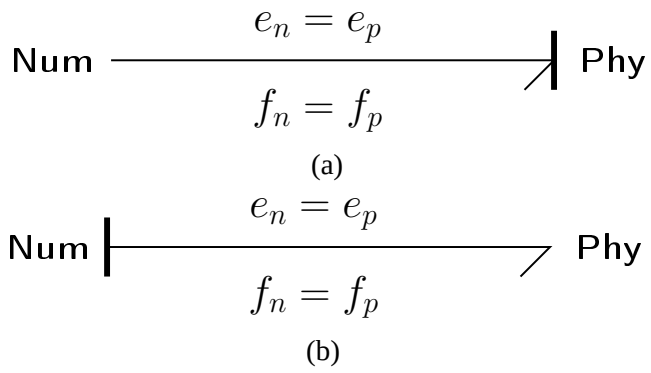

Fig. .2. Causality. (a) Effort actuation. (b) Flow actuation. Note that in the case of (a), the causal strokes imply that e_p is caused by e_n ($e_p := e_n$) but that f_n is caused by f_p ($f_n := f_p$; the reverse is true for (b).

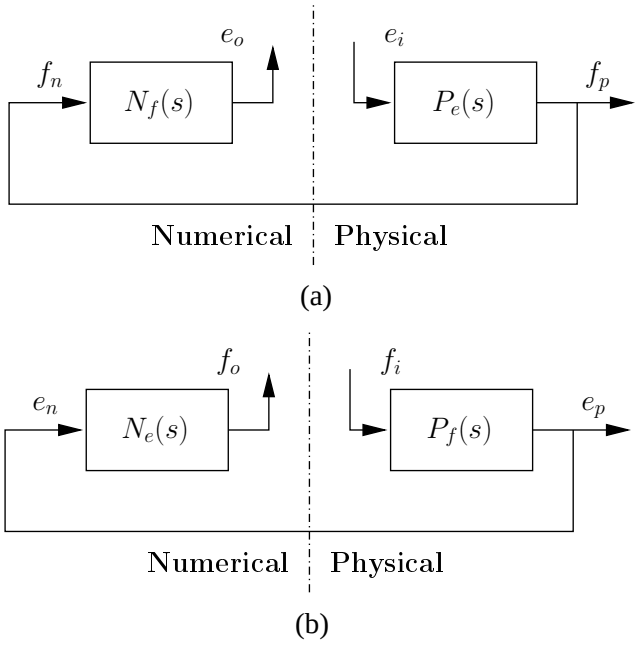

Fig. .3. Block diagrams. (a) Effort actuation, (b) flow actuation.

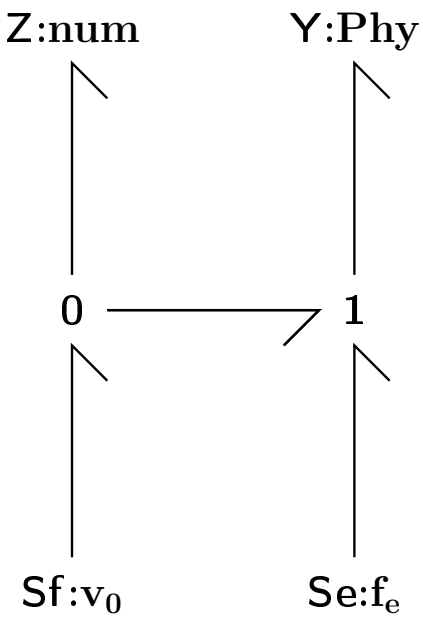

Fig. .4. Impedance control

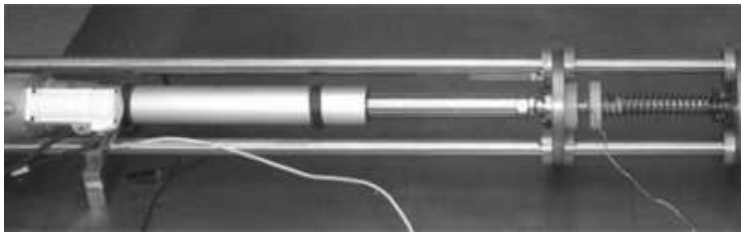

(a)

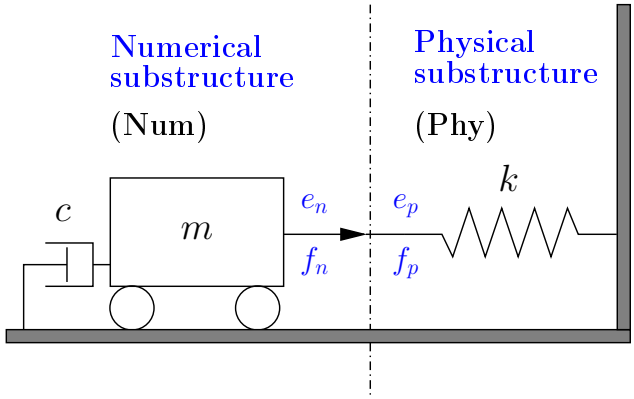

(b)

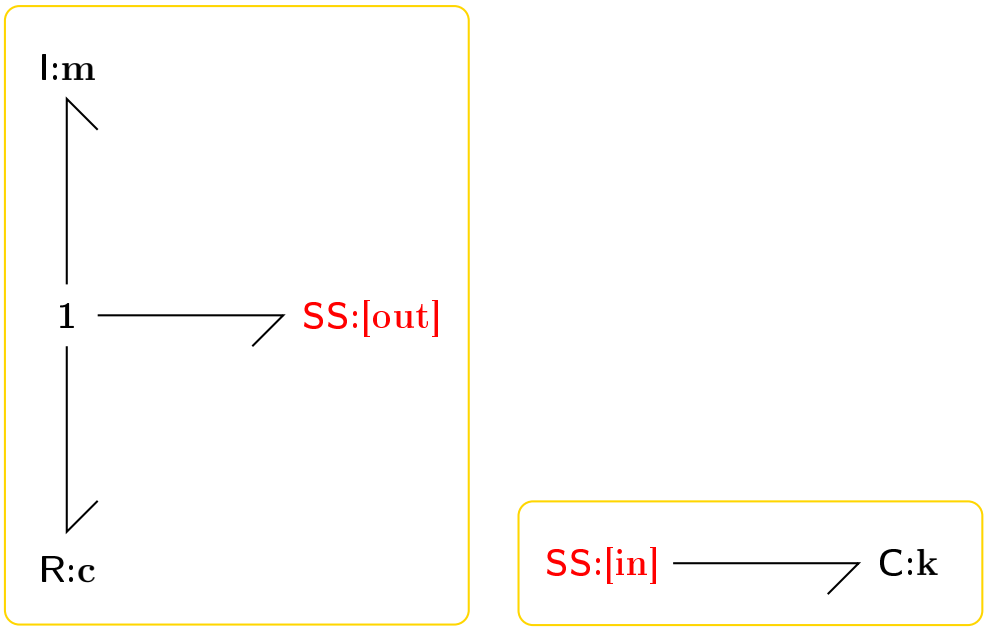

(c) (d)

Fig. .5. Substructuring Example. (a) Photograph, (b) schematic, (c) bond graph of numerical subsystem, (d) bond graph of physical subsystem.

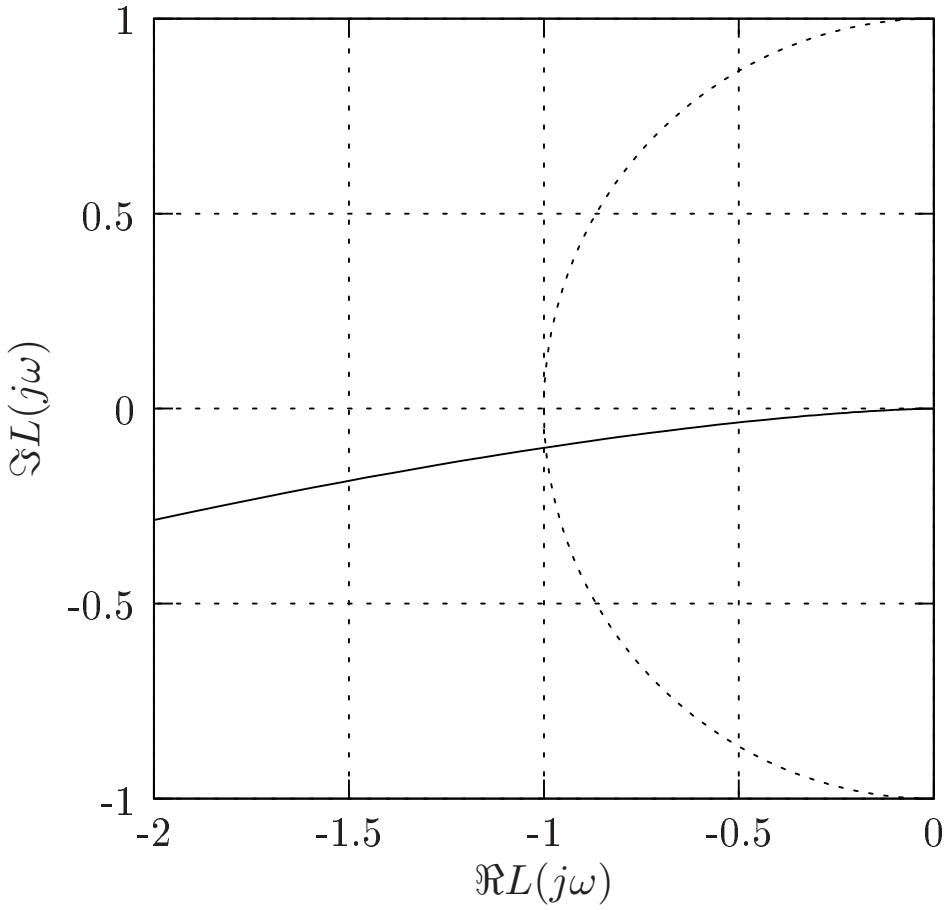

Fig. .6. Substructuring. Nyquist plot with $\zeta = 0.05$, $\phi_m = 6^o$

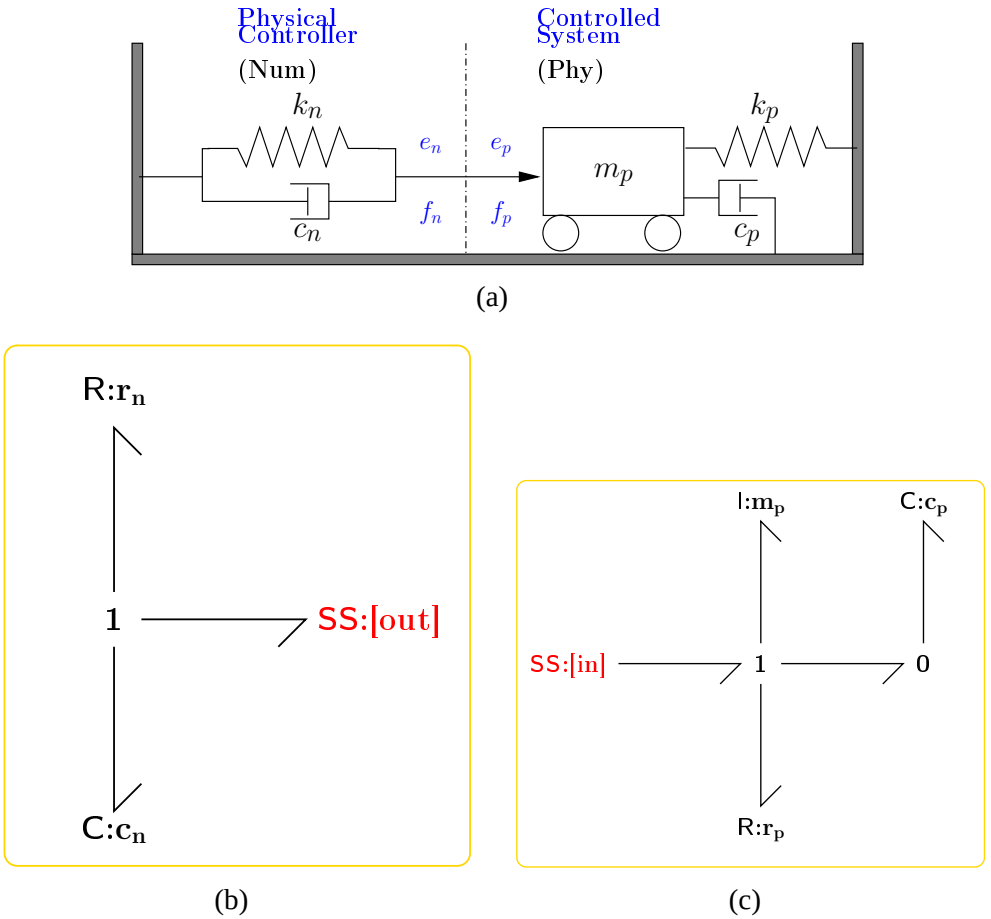

Fig. .7. PMBC example. (a) Schematic, (b) numerical substructure: bond graph, (c) physical substructure: bond graph

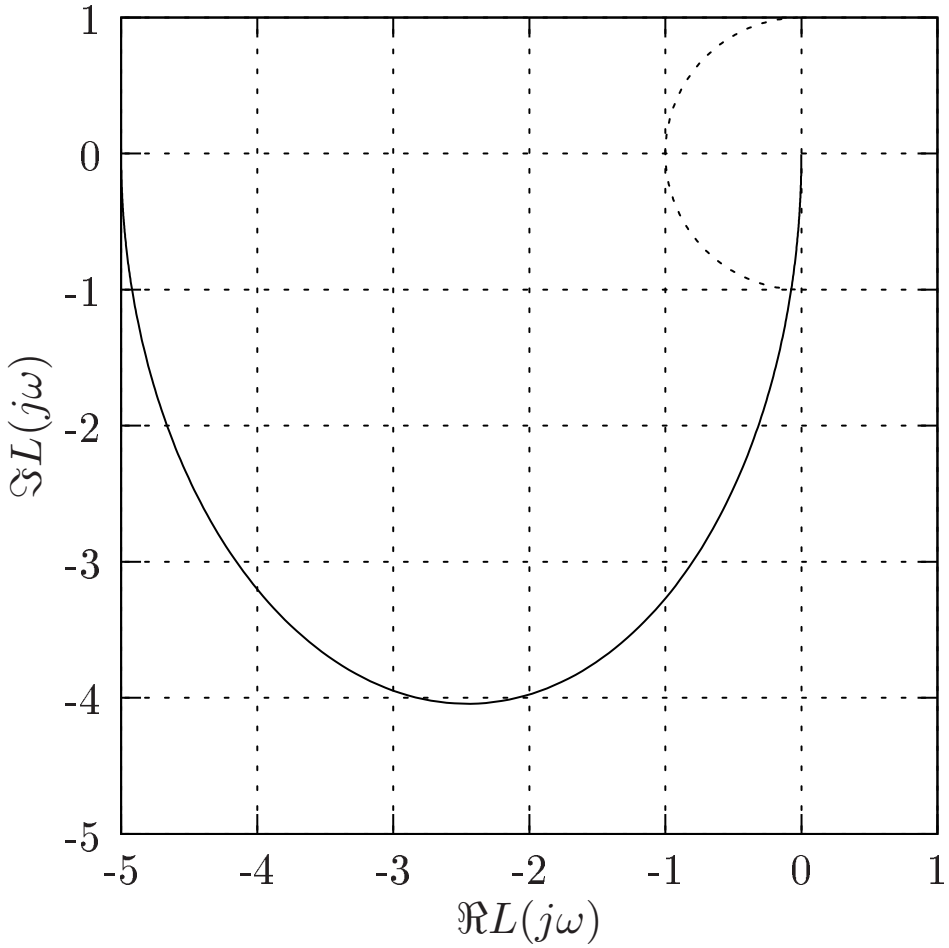

Fig. .8. PMBC: Nyquist plot

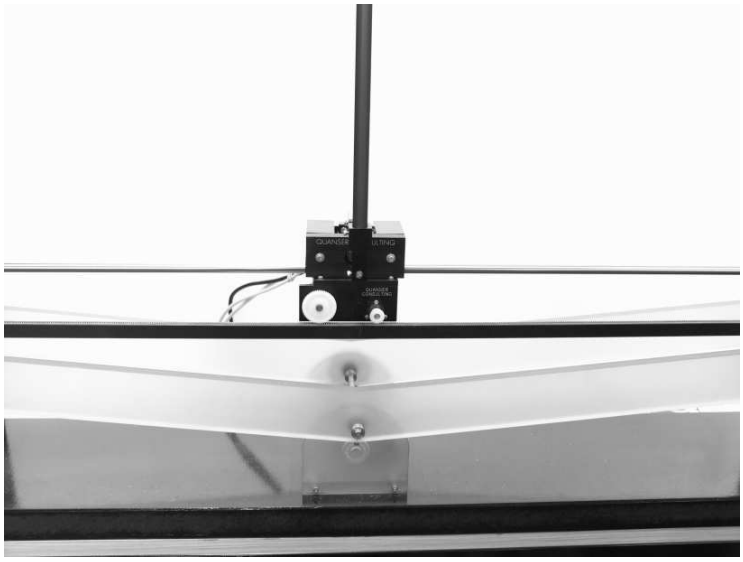

(a)

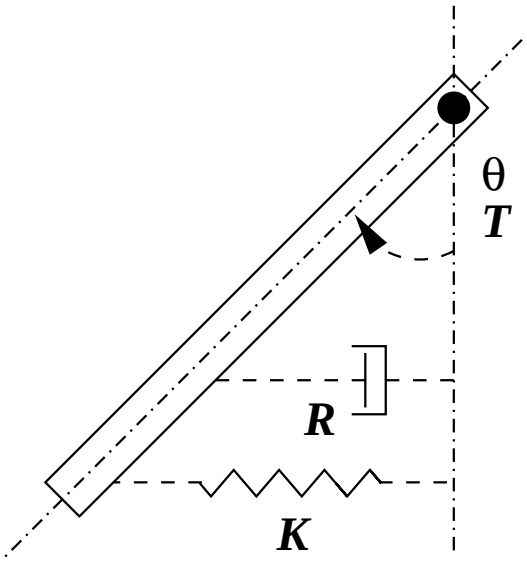

(b)

Fig. .9. Experimental Inverted Pendulum. (a) Photograph, (b) schematic.

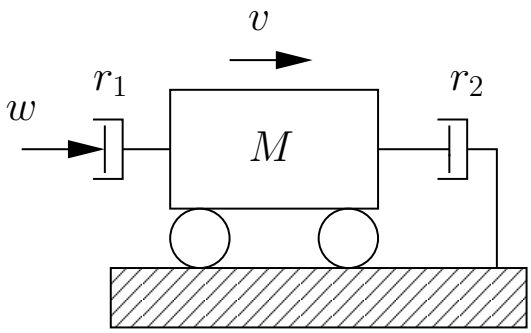

(a)

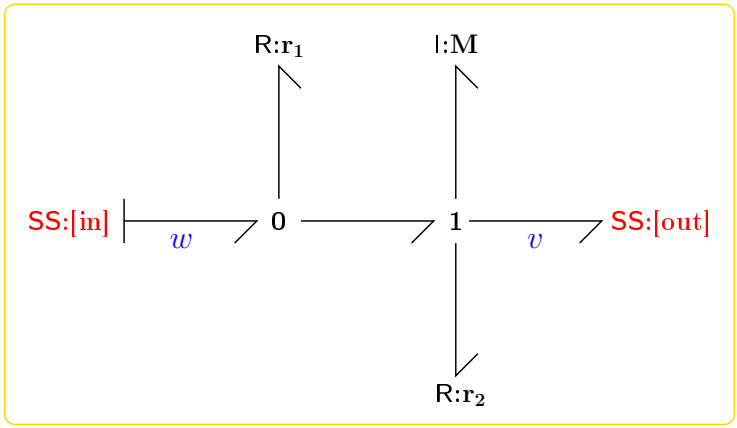

(b)

Fig. .10. Transfer System

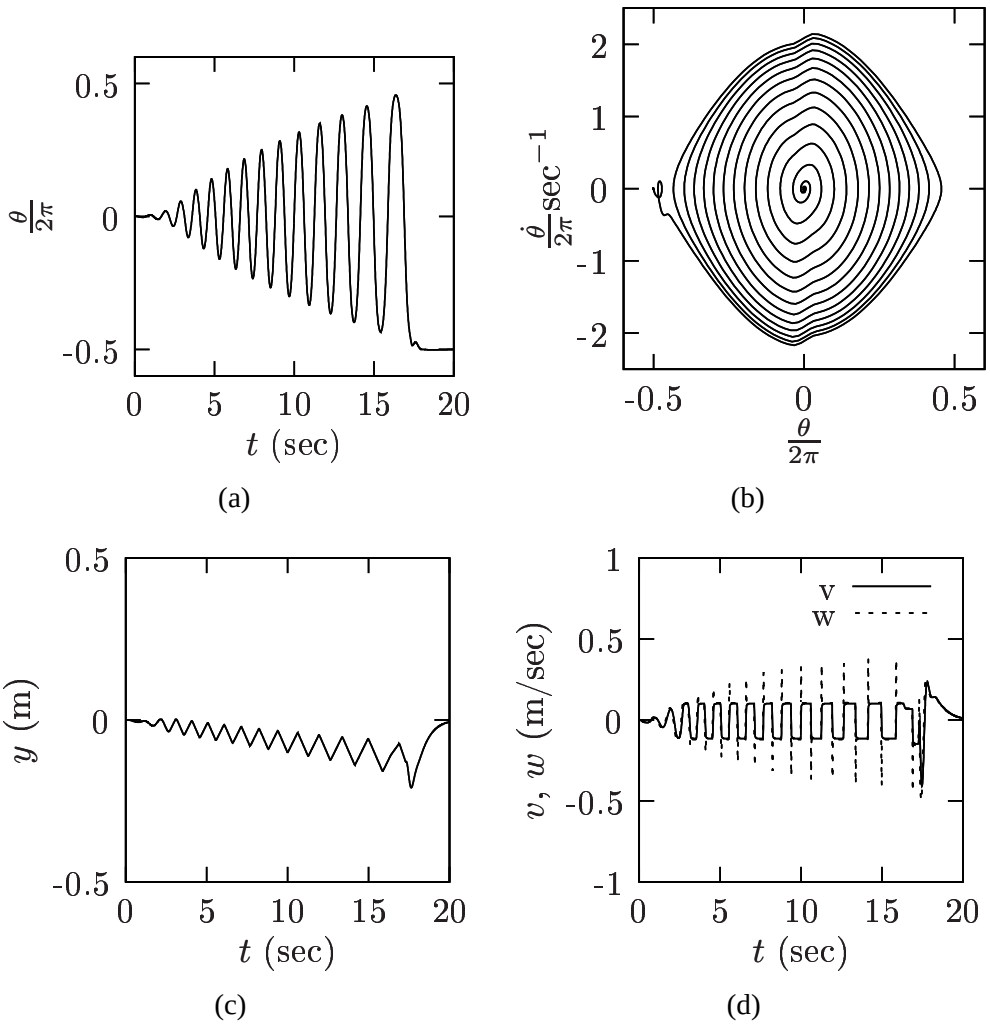

Fig. .11. Simulation results. (a) Pendulum angle θ v. time t, (b) Phase-plane: pendulum velocity $\dot{\theta}$ v. pendulum angle θ, (c) Cart position y v. time t, (d) Cart velocity v v. time t.

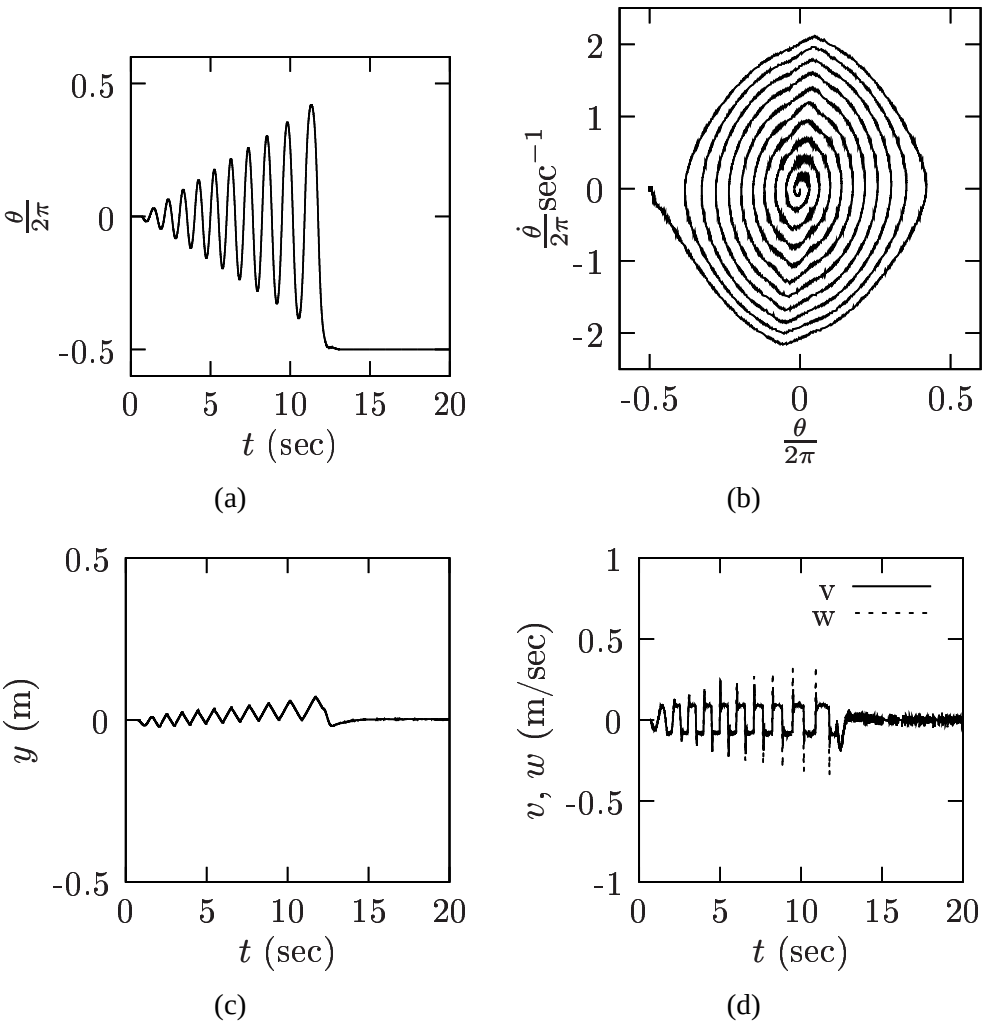

Fig. .12. Experimental results. (a) Pendulum angle θ v. time t, (b) Phase-plane: pendulum velocity $\dot{\theta}$ v. pendulum angle θ, (c) Cart position y v. time t, (d) Cart velocity v v. time t.

List of Tables

k_n	0.8498
c_n	0.1018
k_p	-0.1700
c_p	0.0
m_p	0.003814

Table .1
PMBC parameters

k_u	ζ_u	k_d	ζ_d	α	θ_0
4	1	1	0.2	25	0.2

Table .2
Control parameters

Mkg	r_1Nm^{-1}s	r_2Nm^{-1}s
0.815	19.28	0.86

Table .3
Inner loop parameters